SECRET

UCRL 6238
Cy 135 A

UNCLASSIFIED

MASTER

UNIVERSITY OF CALIFORNIA

CLASSIFICATION CANCELLED

DATE NOV 26 1973

For The Atomic Energy Commission

Bram C. Feldman

Bram C. Feldman
Chief, Reactor, Space and Technology Branch
Division of Classification

Ernest O. Lawrence Radiation Laboratory

AEC RESEARCH AND DEVELOPMENT REPORT

RESTRICTED DATA

This document contains restricted data as defined in the Atomic Energy Act of 1954. Its transmittal or the disclosure of its contents in any manner to an unauthorized person is prohibited.

LIVERMORE SITE

UNCLASSIFIED

SPECIAL REREVIEW FINAL DETERMINATION
Class: U
Reviewers: TR
Class: U
Date: 4-14-82

1 4829

SECRET

DISTRIBUTION OF THIS DOCUMENT IS UNLIMITED

UCRL-6238
Nuclear Rocket &
Ramjet Engines, C-86
M-3679 (24th Ed.)

This document contains 40 pages.
This is copy 135 of 179 Series A.

UNIVERSITY OF CALIFORNIA

Lawrence Radiation Laboratory

Livermore, California

Contract No. W-7405-eng-48

APPLICATION AND EVALUATION OF CERAMIC MATERIALS IN TORY REACTOR SYSTEMS

(Classification of title: Unclassified)

J. H. Moyer, W. B. Myers, C. E. Walter,

and W. M. Wells, Jr.

November 30, 1960

This paper was prepared for presentation at the National Academy of Science, Materials Advisory Board, Symposium on Design With Brittle Materials, held in Washington, D.C., December 13-14, 1960.

BLANK PAGE

DISTRIBUTION

Series A

	Copy No.
LRL Livermore,	
Information Division	1 - 40
Harold Brown	41
John S. Foster	42
C.M. Van Atta	43
Gerald W. Johnson	44
Theodore C. Merkle	45 - 49
Harry L. Reynolds	50
Richard P. Connell	51
James W. Bell	52
Roger E. Batzel	53
Albert J. Kirschbaum	54
Henry C. McDonald, Jr.	55
W. Blake Myers	56 - 60
Carl E. Walter	61 - 62
Jerauld H. Moyer	63
Albert J. Rothman	64
James S. Kane	65
William C. Grayson, Jr.	66
LRL Berkeley,	
Wallace B. Reynolds	67
Hayden S. Gordon	68
LRL Mercury, Nevada,	
James L. Olsen	69
Division of Military Application, Washington,	
Brig. Gen. A.D. Starbird	70
U.S. Atomic Energy Commission, Washington,	
Irving Hoffman	71 - 72
Air Force Special Weapons Center	73
Air Research and Development Command (RDRAP)	74
Air Research and Development Command (RDRRA)	75
Air Technical Intelligence Center	76
Air University Library	77

DISTRIBUTION (Continued)

Series A

	Copy No.
Albuquerque Operations Office	78
Advanced Research Projects Agency	79
Argonne National Laboratory	80
Army Ballistic Missile Agency	81 - 82
Assistant Secretary of Defense, R&D (WSEG)	83
Atomic Energy Commission, Washington	84 - 87
Atomics International	88
Battelle Memorial Institute	89
Brookhaven National Laboratory	90
Bureau of Naval Weapons	91 - 94
Bureau of Naval Weapons (SPO)	95
Bureau of Ships	96
Chicago Operations Office	97
Defense Atomic Support Agency, Sandia	98
Defense Atomic Support Agency, Washington	99
duPont Company, Aiken	100
General Electric Company (ANPD)	101 - 103
General Electric Company, Richland	104 - 105
Lockland Aircraft Reactors Operations Office	106
Los Alamos Scientific Laboratory	107 - 108
Marquardt Corporation	109
National Aeronautics & Space Administration, Cleveland	110 - 111
National Aeronautics & Space Administration, Washington	112 - 113
New York Operations Office	114
Oak Ridge Operations Office	115
Office of Naval Research	116
Office of the Assistant for Operations Analysis DCS/O	117
Office of the Chief of Naval Operations	118
Patent Branch, Washington	119
Phillips Petroleum Company (NRTS)	120
Pratt and Whitney Aircraft Division	121
San Francisco Operations Office	122

DISTRIBUTION (Continued)

Series A

	Copy No.
Sandia Corporation	123
School of Aviation Medicine	124
Union Carbide Nuclear Company (ORNL)	125
USAF Project RAND	126 - 127
U. S. Naval Postgraduate School	128
Wright Air Development Division	129 - 134
Office of Technical Information Extension	135 - 179

BLANK PAGE

CONTENTS

Page No.

Abstract 9

I. Introduction 11

II. Reactor and Environment 11

III. Tory Reactors 12

A. Tory II-A 13

B. Tory II-C 14

IV. Thermal Stress Analysis and Tests 15

V. Ceramic Domes 17

VI. Test Results on Mechanical Behavior of Dome Structures . 17

VII. BeO Properties Pertinent to Ramjet Reactor Design . . 19

A. Modulus of Rupture of $BeO-UO_2$ Fuel Tubes 19

B. Modulus of Rupture of Tory II-A Dogbones 20

C. Effects of Irradiation on $BeO-UO_2$ 20

D. Typical Creep Data on BeO 21

References 22

BLANK PAGE

APPLICATION AND EVALUATION OF CERAMIC MATERIALS IN TORY REACTOR SYSTEMS

J.H. Moyer, W.B. Myers, C.E. Walter,
and W.M. Wells, Jr.

Lawrence Radiation Laboratory, University of California
Livermore, California

ABSTRACT

The Tory series of test reactors is intended to lead to a reactor capable of use as a ramjet power plant. Current designs are presented. Beryllium oxide is presently the only serious contender as the moderator. Analytical and experimental treatment of the thermal stress problem in BeO is discussed. There is a requirement that a ramjet reactor sustain very large forces caused by flow-induced pressure drop. Development of ceramic structural elements to sustain these forces is discussed.

BLANK PAGE

APPLICATION AND EVALUATION OF CERAMIC MATERIALS IN TORY REACTOR SYSTEMS*

J.H. Moyer, W.B. Myers, C.E. Walter,
and W.M. Wells, Jr.

Lawrence Radiation Laboratory, University of California
Livermore, California

I. INTRODUCTION

Lawrence Radiation Laboratory is currently engaged in the development of a reactor for a supersonic low-altitude nuclear ramjet. This project is named Pluto by the Atomic Energy Commission. The term SLAM, which is an Air Force contractor's designation for a complete ramjet missile system using the Pluto reactor, is also a familiar one. The test reactors being developed at LRL have been dubbed Tory.

II. REACTOR AND ENVIRONMENT

The SLAM mission concept, briefly, is to come in on target while flying near Mach 3 "on the deck" to avoid early detection. This mission concept, coupled with consideration of aerothermodynamics, neutronics, payload volume, and material properties serves to establish within fairly narrow limits the size, temperature, material, and porosity of the reactor. Such a study results in requirements for the reactor which cannot deviate greatly, in the present state of technology, from those given in Fig. 1.

Delete for CAP 7/2/62

*Work done under the auspices of the U.S. Atomic Energy Commission.

The moderator choice is rapidly narrowed down by neutronic considerations to materials containing Be and C. The presence of air, the high temperature involved, and the choice of neutronically acceptable compounds of these elements leave only BeO as a suitable choice. Beryllides show promise but their technology is yet young.

It has been found feasible to disperse a uranium compound in BeO to the extent required by criticality. The maximum loading required is about 8 percent by weight. An intensive effort is being expended to improve the properties of BeO + $U^{235}O_2$ material at LRL. High density and purity sintered shapes are currently being produced at LRL. The fueled BeO process development has led to an extruded hexagonal fuel element. Its basic size is 0.3 in. flat-to-flat with a 1/4-in.-diam axial hole and 4 in. long. A flying reactor requires about half a million of these tubes. The chosen size is a compromise among the competing requirements: enhancement of performance, reduction of thermal stress, ease of assembly, and economical fabrication.

The radial temperature profile is flattened by varying the uranium concentration radially. The overall axial temperature difference shown in Fig. 2 is the same as the air temperature difference, or about 1100°F in 5 feet. The axial profile is not linear and has severe discontinuities at the reflector interfaces.

The environment indicated in Figs. 1 and 2 poses no easy problem in holding together a multipiece ceramic reactor having these characteristics.

III. TORY REACTORS

To develop a flyable reactor LRL is now fielding a test reactor, designated Tory II-A, at the AEC's Nevada Test Site. In about two years a prototype designated Tory II-C, which would actually be capable of flying given a suitable airframe, will be tested at the same site. Time permits only a brief description of these reactors.

A. Tory II-A

Figures 3 and 4 show the Tory II-A reactor. The ceramic core was reduced in diameter to conserve ceramic cost. Criticality is achieved by surrounding the core pressure vessel with a water-cooled graphite reflector. Control is accomplished in the reflector.

The ceramic tubes are separated into modules and supported laterally by BeO structural links. Alignment of flow holes is maintained by staggering the ends of the tubes. The eyes of the structural links are threaded on cooled metal tie tubes which run the length of the core in a hexagonal array. The tie tubes are attached to a metal grid in front of the core and support a refractory metal plate at the back of each module.

With this design, the pressure drop caused by air flow through the reactor is resisted by the refractory metal base plates and transmitted to the front support grid by the tie tubes. Because the reactor is tested in a horizontal position, the structural BeO links (or dogbones) support the weight of the associated bundle of ceramic tubes. This load is carried in bending by the dogbones and the metal tie tubes. Photoelastic stress analysis of the dogbones indicates that bending stresses are low. Each dogbone was carefully inspected for flaws before assembly of the core.

By grouping the ceramic tubes into modules the problem associated with thermal expansions was minimized. This is indeed a problem, particularly when one considers the large temperature (and hence expansion) discontinuities at the front reflector interface. The disadvantage lies in the relatively great fraction ($\approx$ 18%) of the core volume taken up nonproductively by unfueled BeO in the dogbones, tie tubes, and incidental void.

B. Tory II-C

Two designs are in progress involving high productive volume ratios. The first one, shown in Fig. 5, utilizes the same primary structure as in Tory II-A except that the brittle dogbones have been eliminated. Instead, lateral loads of the magnitude expected in flight are transmitted through a close packed array of the ceramic tubes to a peripheral spring support system. Again the ends of the tubes are staggered, in this case to eliminate cleavage planes as well as to provide flow hole alignment. The side support components are cooled by inlet ram air.

The side support system allows different thermal expansion of the reactor at different axial stations. The large expansion discontinuity at the front reflector interface (referring to the temperature profile of Fig. 2) has been solved in this design as shown in Fig. 6, by allowing the bank of reflector tubes next to the active core to act as round end columns. These column tubes are not supported laterally by side springs. Alternate tubes extend sufficiently into the adjacent banks of tubes to be supported by them.

In the second Tory II-C design the tie tubes and refractory metal base plates are eliminated. The axial thrust loading on the reactor is resisted by a large ceramic dome as shown in Fig. 7. This design results in a considerable economy of neutrons since the space left by the tie tubes is occupied by fueled ceramic tubes. This design is aimed at allowing higher temperatures.

Both designs for Tory II-C have internal cavities for control rods. The presence of control rods causes severe flux perturbation in adjacent ceramic tubes. Careful consideration of this perturbation is required as it affects the thermal stress in the ceramic tube.

IV. THERMAL STRESS ANALYSIS AND TESTS

There is a particular interest in the thermal stresses in the ceramic fuel tubes. It can be shown that, for the purpose of thermal stress analysis, a hexagonal tube with an axial circular hole is closely approximated by a circular tube having the same hole diameter and total cross-sectional area.[1]

If the material of the ceramic fuel tube remains elastic, the maximum thermal stress is given by:

$$\sigma = \left(\frac{E\alpha}{k}\right) Qa^2\psi , \tag{1}$$

where

σ = maximum thermal stress

E = Young's modulus

α = instantaneous coefficient of thermal expansion

k = thermal conductivity

Q = uniform volumetric heat generation rate in material

a = hole radius

ψ = dimensionless function of porosity and Poisson's ratio.

This is a biaxial stress which is tensile at the inside surface of the tube. The tensile stress in the equivalent hexagonal tube is a few percent higher near the ends.

Substitution in Eq. (1) of numerical values appropriate for the Tory reactors proves to be discouraging. For example, as noted subsequently, the mean short time modulus of rupture of BeO + $U^{235}O_2$ from one supplier at 2400°F is 12,500 psi. Yet Eq. (1) yields an elastic stress of 28,000 psi!

Fortunately, it is apparent from simulation experiments that the ceramic tubes do not break under expected reactor conditions. Work is now underway to study the inelastic action to which this anomaly must be attributed.

Equation (1) may be rewritten in a particularly convenient manner:

$$\frac{\sigma k}{E\alpha} = Qa^2\psi \text{ watts/in.} \qquad (2)$$

In Eq. (2) the right hand side may be evaluated without regard to material properties. For example, its peak value in the Tory II-C reactor is 17.7 watts/in.

The fact that expressions for elastic thermal stresses are used means only that they are a convenient means of data presentation. As pointed out above, they are known not to be precise for the materials and conditions at hand.

In the simulation experiments, because it is impractical to generate heat within the ceramic tube, heat is radiated to its outer surface. The heat is transferred through the tube wall to gas flowing through the tube. An expression similar to Eq. (2) and containing the quantity $\sigma k/E\alpha$ can be derived for elastic thermal stresses in this situation. Thus, experiments can be conducted for values of $\sigma k/E\alpha$ which are of interest in the Tory reactors. The experiments were performed in a facility named Blowpipe.

Figure 8 presents some data from Blowpipe. The lower curve represents the calculated values of $\sigma k/E\alpha$ for Tory II-A. The numbers along the curve indicate relative axial position. Fourteen tests yielding conditions in the hatched area produced relatively minor cracking in four tubes. The remaining ten were undamaged. The specimens were BeO-UO_2 with the weight percent of UO_2 varying between 5.3% and 7.0%. They were produced at LRL and had nominal dimensions as shown in the figure. An appreciable quantity of data is not included because pretest calibration procedures heated specimens to temperatures in excess of the sintering temperatures.

V. CERAMIC DOMES

The most critical item in the second Tory II-C design is the large ceramic dome. A dome appropriate for Tory II-C-2 is shown in Fig. 9. Since the dome is essentially in compression, allowable stresses can be considerably greater than tensile strength would dictate. A review of the properties of relatively pure high-density ceramics and cheaper grades of refractories indicates that several materials could compete for this application. Silicon carbide was selected for thorough evaluation because of several desirable properties. SiC can be relatively easily fabricated. KT SiC (Carborundum Company) is cold pressed. It can be easily machined before firing, and because of uniquely low shrinkage (less than 1%) it should require little or no final machining. The firing operation involves chemical changes and consequently differs from the normal sintering procedure. In this case where the temperature differences are fixed by the flowing air the product $E\alpha$ indicates the thermal stress behavior. The product $E\alpha$ for SiC is about a factor of 3 lower than Al_2O_3 or BeO.

Since the dome is in compression it need not be monolithic. In fact, should the dome crack, failure would not be imminent. The first intermediate-scale dome will be composed of seven pieces. Pieces of the required size for this are currently being fabricated at Carborundum Company.

VI. TEST RESULTS ON MECHANICAL BEHAVIOR OF DOME STRUCTURES

Three types of tests dealing with mechanical behavior of domes have been conducted. All tests deal with small-scale models and rely on the scaling prediction that stresses are conserved for a given applied pressure regardless of the linear scale of the structure. The three types of tests and results are as follows:

1. Photoelastic stress analysis of unperforated domes. Figure 10 shows the variation of surface stress in a radial plane. The stress plotted is the compressive stress tangent to the surface at the point plotted. These stresses have been normalized to the applied pressure. The model diameter was 12 in. and the technique was the "frozen stress" procedure.

The results serve to support calculations and intuition to the effect that stresses in these kinds of configurations are largely compressive and that the stress values are low. In order to get an indication of the stress levels in a perforated dome, the values in Fig. 10 should be multiplied by the ratio of hole spacing to web thickness. This ratio is about 4 or 5 for interesting geometries. Data on circumferential stresses were not available in time for inclusion here.

2. Perforated plaster-of-Paris domes. Eight 12-in. domes perforated with 1/2-in. holes to 50% void fraction were tested to destruction under hydrostatically applied load. Two primary conclusions may be drawn from these data:

a) Plaster-of-Paris domes were able to sustain flat face pressures almost equal to that required in the application. Figure 11 shows load deflection data for the eight domes. Six were one-piece domes and two were seven-piece domes. The plaster of Paris has a compressive strength of about 2500 psi. Using this compressive strength and the photoelastic results, one can predict the failures fairly well. The Carborundum Company's KT silicon carbide has a compressive strength of the order of 100,000 psi at temperatures of interest.

b) The dome configuration and the attendant compressive stresses can allow load to be sustained after severe cracking of the dome. Figure 12 is a photograph of the under surface of a dome while it is sustaining the maximum pressure. The cracks had all occurred earlier. Figure 13 shows the same dome after unloading and after the pieces had been separated by hand.

3. 3-1/2-in. silicon carbide domes. Figure 14 shows an apparatus for testing 3-1/2-in.-diam domes at elevated temperature. The tests were conducted in an argon atmosphere to avoid oxidation of the molybdenum parts. The results are summarized in Table I.

Table I. High-temperature dome test data.

	Temp	Pressure on flat face	Time
SiC dome No. 1	2200°F	300 psi	2 hr 57 min
	"	1000 "	2 hr 30 min
	"	1130 "	1/2 min
SiC dome No. 2	2350°F	1000 "	2 hr 12 min

Some cracking was observed after the pieces were removed from the test fixture; however, rough handling was required for disassembly because parts of the test fixture bonded to each other. Consequently, there is some uncertainty as to the source of the cracks. In all cases the domes were in one piece after removal from the test fixture. All tests were discontinued because of diaphragm failure.

VII. BeO PROPERTIES PERTINENT TO RAMJET REACTOR DESIGN

A. Modulus of Rupture of $BeO-UO_2$ Fuel Tubes

Figure 15 shows bending strength data for about 300 hexagonal BeO-7.88 wt% UO_2 tubes. These tubes were purchased by LRL from the Aircraft Nuclear Propulsion Division of the General Electric Company as Tory II-A fuel elements. The tubes were loaded in three-point bending as indicated. The stress is calculated with the conventional assumption of linear stress distribution (modulus of rupture). Loading was done in air. The plotted values are maximum stress (at center point).

B. Modulus of Rupture of Tory II-A Dogbones

The flexural strength of unfueled BeO structural links was measured at room temperature and approximately 1900°F. All specimens were inspected before testing by radiographic and fluorescent penetrant methods to insure soundness. Data are shown in Figs. 16 and 17 for material produced by two manufacturing methods.

These tests were made by bending the bar in three-point loading and breaking the eye by loading along a diameter. Maximum stress was computed elastically for the web fracture. Stress in the eye was related to applied force by a photoelastic study.

C. Effects of Irradiation on BeO-UO_2

The observed effect of reactor radiation on BeO containing UO_2 that has aroused most concern has been the effect on thermal conductivity. There are direct implications with respect to thermal stress.

Data obtained by Argonne National Laboratories[2, 3] in 1946 showed large changes in thermal conductivity. Post-irradiation annealing removed some of the change, but post-annealing ceased to be effective above 1000°C (as explicitly stated in ref. 2).

The data are plotted in Fig. 18 as k_0/k (the initial conductivity to final conductivity ratio) vs temperature of the post-irradiation anneal. The irradiations were carried out at about 650°C on BeO-10 wt% UO_2 in vacuo. The Argonne irradiations were conducted to integrated dosages of about .6 kw-hr/cm^3.

Also plotted are two points obtained at LRL[4] on BeO-5.8 wt% UO_2. The difference in test procedure is that the LRL data are obtained with irradiation at 1335°C. The point indicating no change in conductivity had an integrated dosage of about 0.6 kw-hr/cm^3, and the point showing a 10% change has an integrated dosage of 6 kw-hr/cm^3. The larger dosage and the temperature are representative of the maximum conditions for a Pluto mission.

The primary conclusion appears to be that the extrapolation of post-annealing data, to the effect that $k_0/k = 2.5$ for temperatures greater than 1000°C does not apply when irradiation is conducted at the temperature of our tests. Temperatures lower than 1335°C will, of course, be present in Pluto reactors, and work is continuing in this area.

D. Typical Creep Data on BeO

A program for measuring compressive creep of BeO is underway at LRL. Figure 19 shows some typical creep data. The specimens were 3/4-in. o.d. by 1/4-in. i.d. by 2 in. long. They were fabricated by extrusion and were tested in air after a period of about one hour to bring to temperature. The densities of the specimens were as follows:

10 wt% UO_2: 99.0% of theoretical
5 wt% UO_2: 98.6% " "
pure BeO: 96.3% " "

More complete data can be found in refs. 5 and 6.

REFERENCES

[1]R. B. Meuser, "Temperatures and Thermal Stresses in Hexagonal Tubes with Internal Heat Sources," Lawrence Radiation Laboratory report UCRL-5692, Sept. 1959.

[2]J. R. Gilbreath and O. C. Simpson, "The Effect of Reactor Irradiation on the Physical Properties of Beryllium Oxide," Second United Nations International Conference on the Peaceful Uses of Atomic Energy (Geneva, 1958), Paper 621, vol. 5, p. 367.

[3]Verbal communication between personnel of Lawrence Radiation Laboratory and Argonne National Laboratory.

[4]H. R. Leider, "The Effect of Reactor Irradiation on the Thermal Conductivity of BeO-UO_2 Specimens," Lawrence Radiation Laboratory report UCRL-5833, Jan. 1960.

[5]"Pluto Quarterly Report No. 4 (April—June 1960)," Lawrence Radiation Laboratory report UCRL-6036, July 1, 1960.

[6]"Pluto Quarterly Report No. 5 (July—September 1960)," Lawrence Radiation Laboratory report UCRL-6143, Oct. 1, 1960.

/md

NUCLEAR RAMJET MISSILE

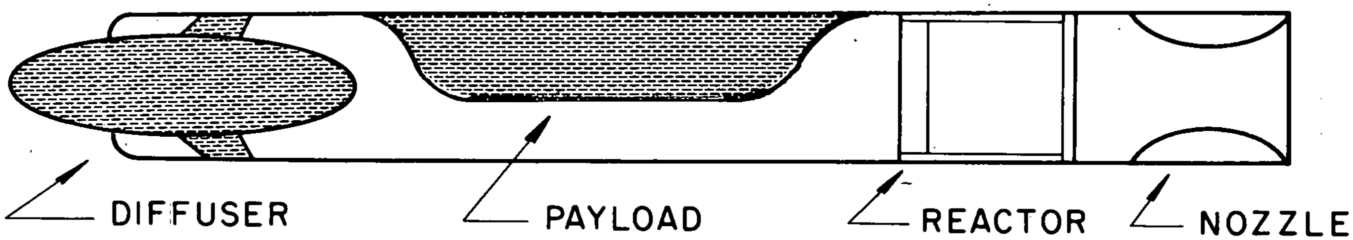

REACTOR CHARACTERISTICS

TYPE	LIGHTLY REFLECTED HOMOGENEOUS CORE
MODERATOR	BeO
FUEL	$U^{235}O_2$ DISPERSED IN BeO
DIAMETER	54 in. } INCL. REFLECTORS
LENGTH	60 in. } INCL. REFLECTORS
POROSITY	50%
L/D FOR HEAT TRANSFER	240

REACTOR ENVIRONMENT

AXIAL & LATERAL FLIGHT LOADS (BOOST, MANEUVER, GUST, etc.)	~5g
AXIAL THRUST LOADING	125 psi
INLET AIR TOTAL TEMPERATURE	1060°F
EXIT AIR TOTAL TEMPERATURE	2180°F
PEAK WALL TEMPERATURE	2500°F
AVE. MATERIAL POWER DENSITY	26 Mw/ft^3
LIFE	3-10 hr
INTEGRATED FLUX (nvt)	10^{19} n/cm^2

MUL-11654

Fig. 1. Requirements for a nuclear ramjet reactor.

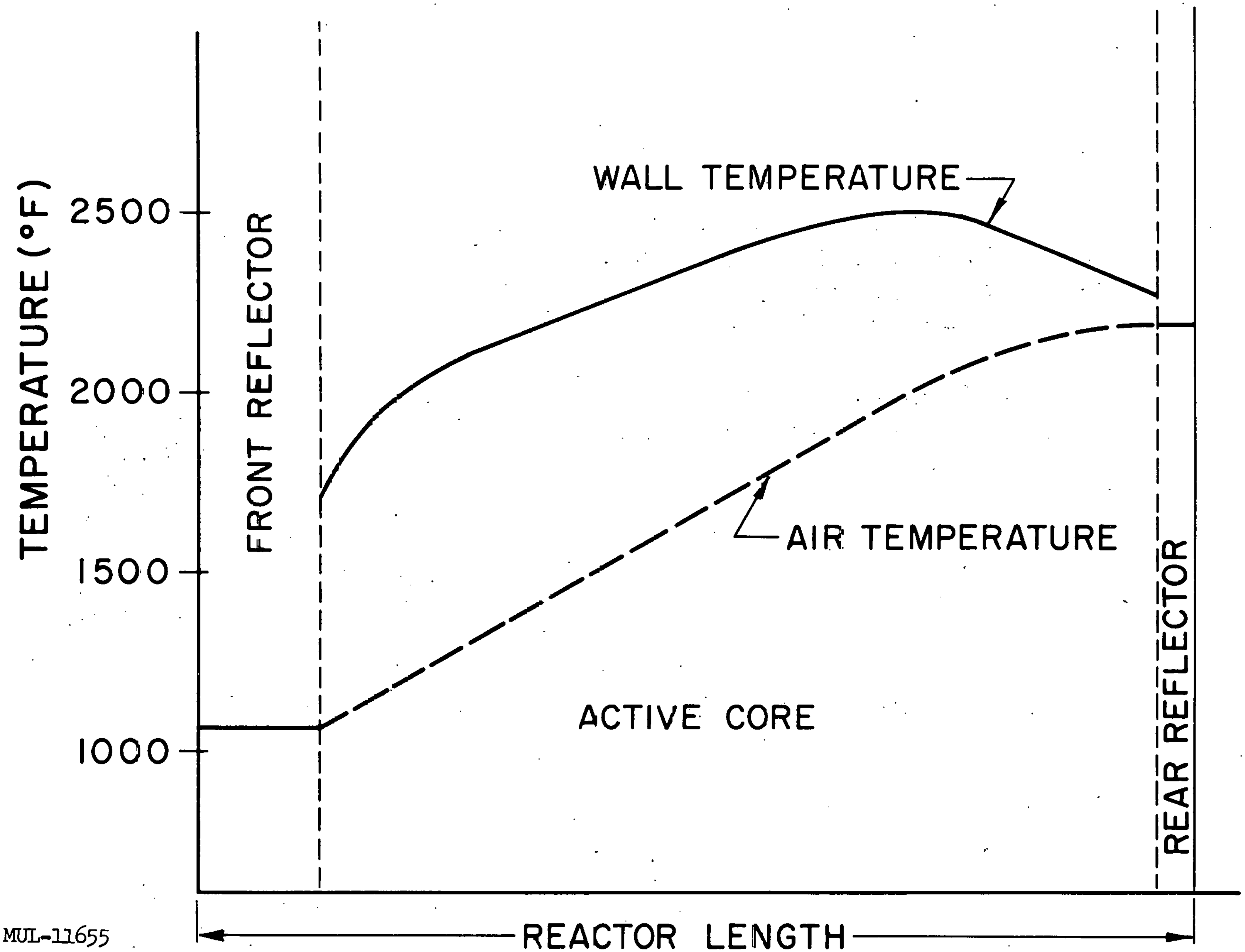

MUL-11655

Fig. 2. Axial wall and air temperature profile.

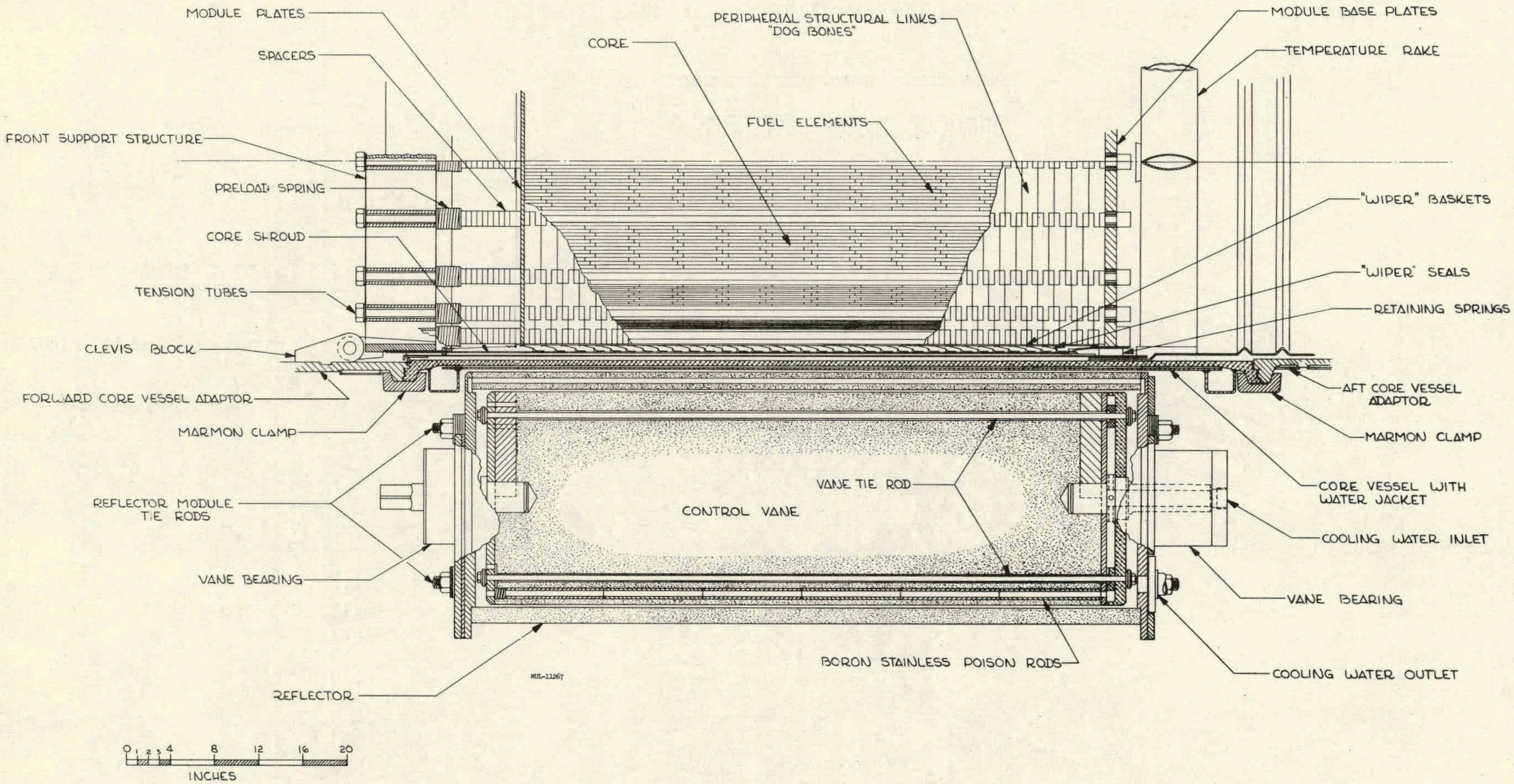

Fig. 3. Tory II-A test reactor.

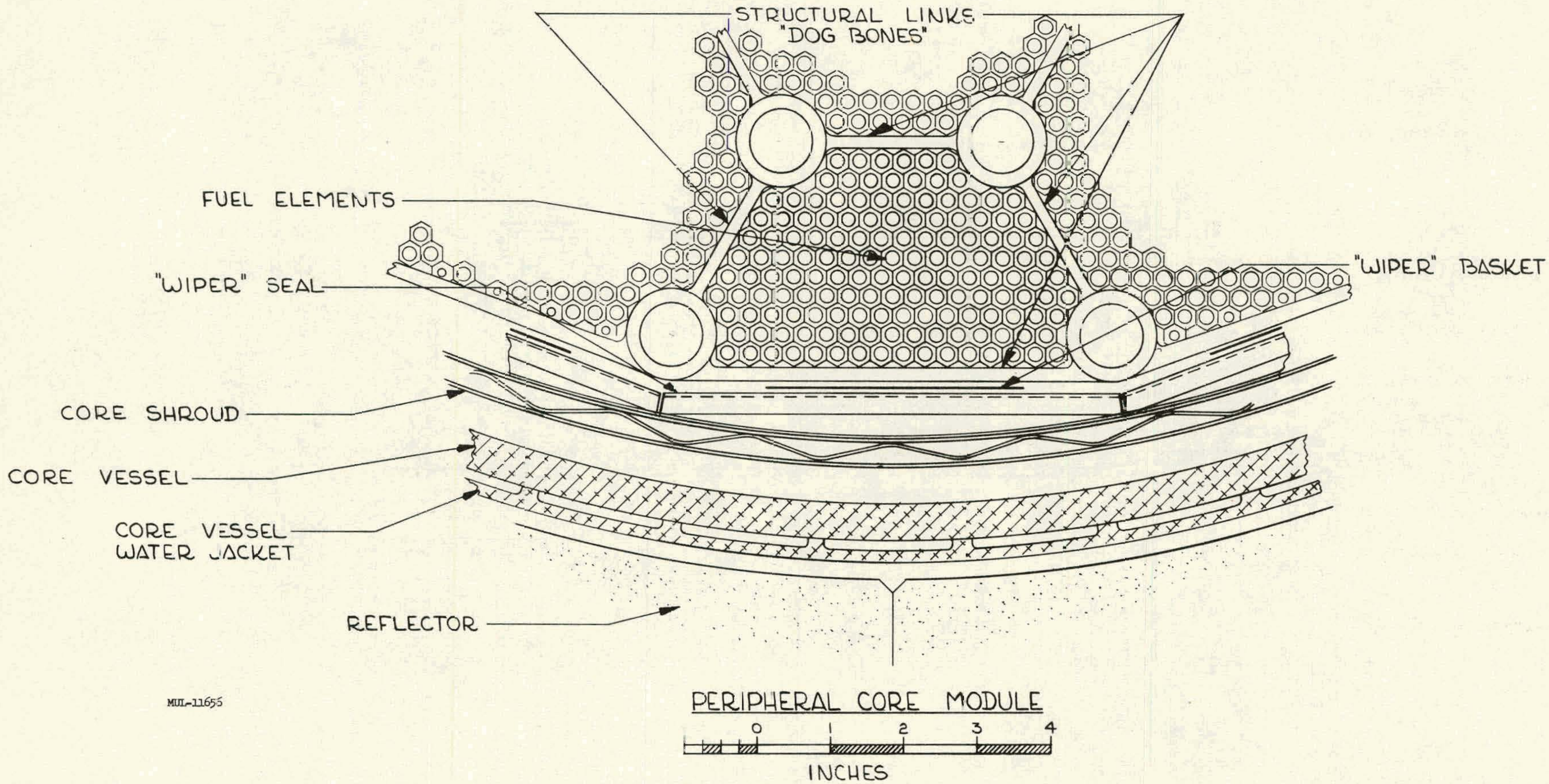

Fig. 4. Tory II-A test reactcr.

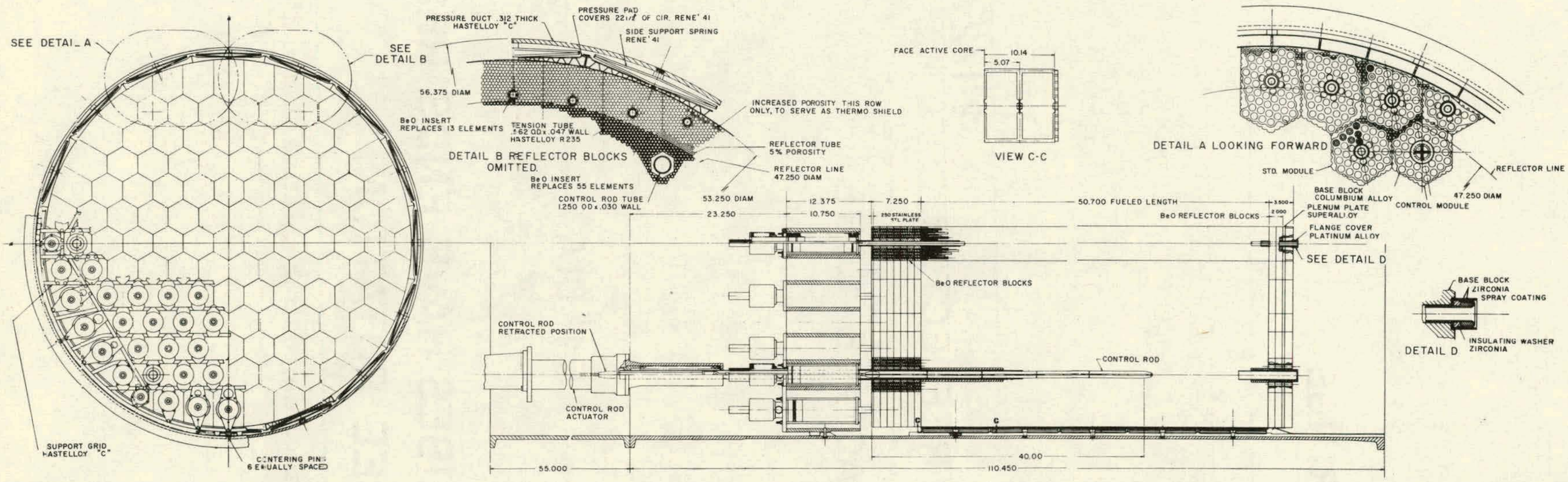

MUL-11231

Fig. 5. Tory II-C-1 test reactor.

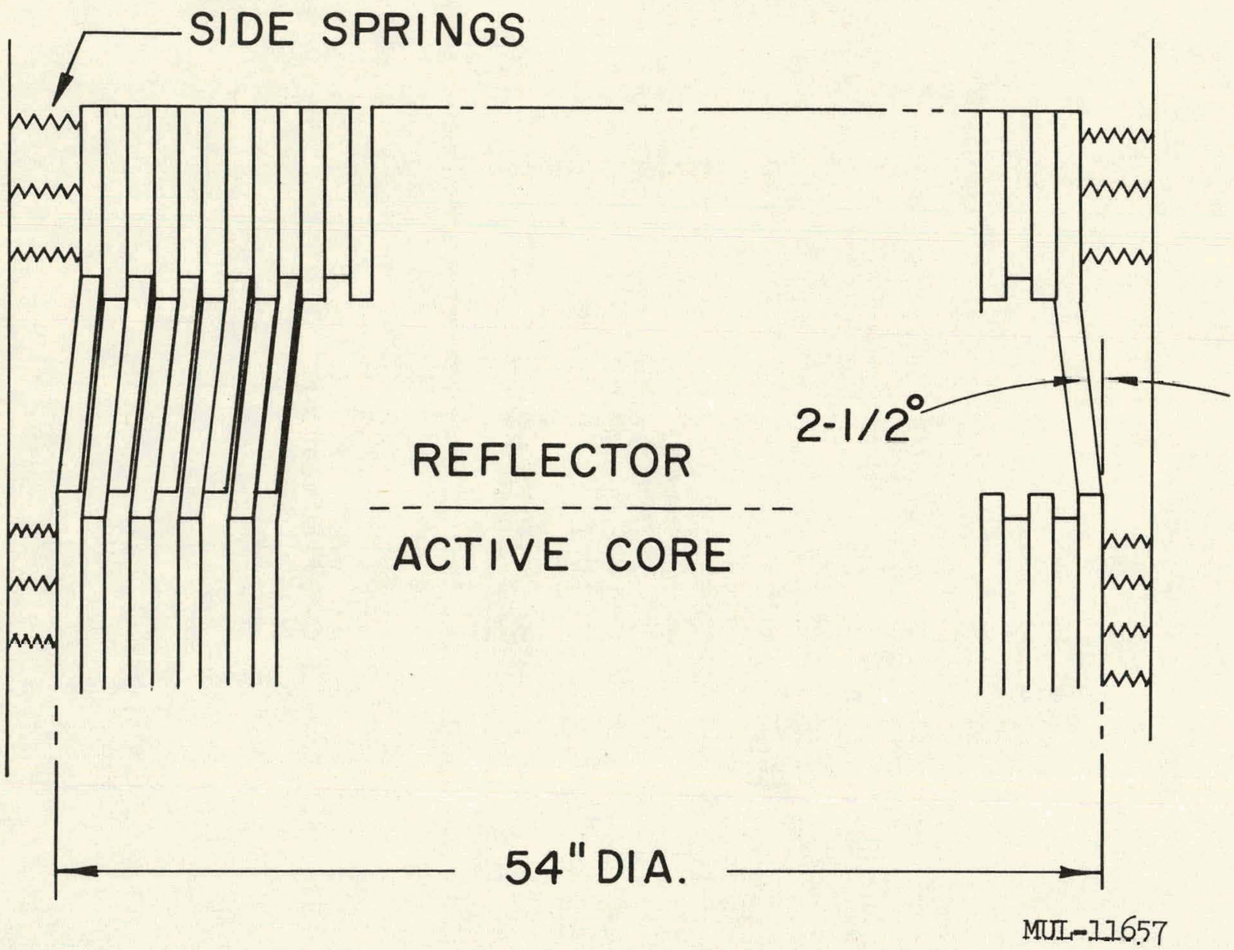

TRANSITION TUBES HAVE ENDS RELIEVED TO PERMIT FREE ROTATION.

Fig. 6. Method of accommodating relative thermal expansion.

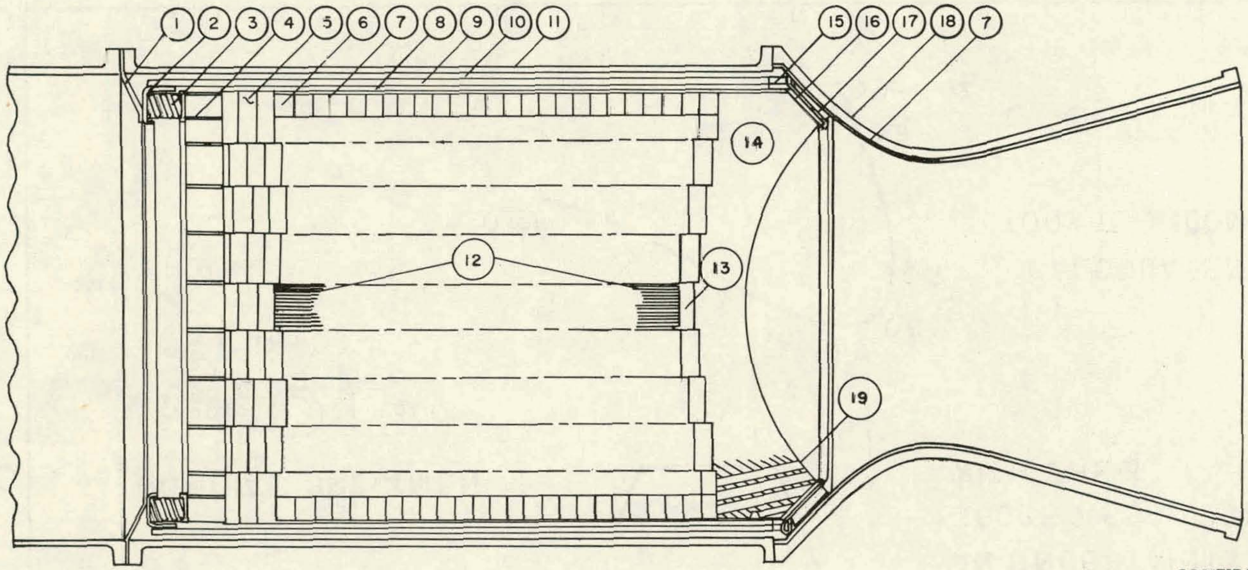

CONFIDENTIAL R D

LEGEND

1 FWD. SHEAR JOINT SUPPORT AND ASSY. PRELOAD RING
2 AXIAL PRELOAD SPRING SUPPORT RING
3 AXIAL PRELOAD SPRING
4 AXIAL PRELOAD GRID
5 FWD. REFLECTOR PIECES
6 SIDE REFLECTOR PIECES
7 FLAME SPRAYED ZrO_2 THERMAL INSULATION
8 REFRACTORY FIBER THERMAL INSULATION (INCONEL FOIL WRAP)
9 CORRUGATED Ni ALLOY GIRDLE
10 RADIAL PRESSURE CONTROL AND BYPASS COOLING AIR ANNULUS
11 PRESSURE VESSEL AND DUCT
12 FUELED MATRIX ELEMENTS
13 TRANSITION PIECE(S)
14 REAR SUPPORT STRUCTURE ("DOME")
15 TOGGLE BOLT (DOME SEAT ATTACH)
16 DOME SEAT
17 DOME SEAT RETAINER AND SUPPORT RING
18 EXIT NOZZLE
19 FLOW DOME PASSAGE

MUL-11216

Fig. 7. Tory II-C-2 test reactor.

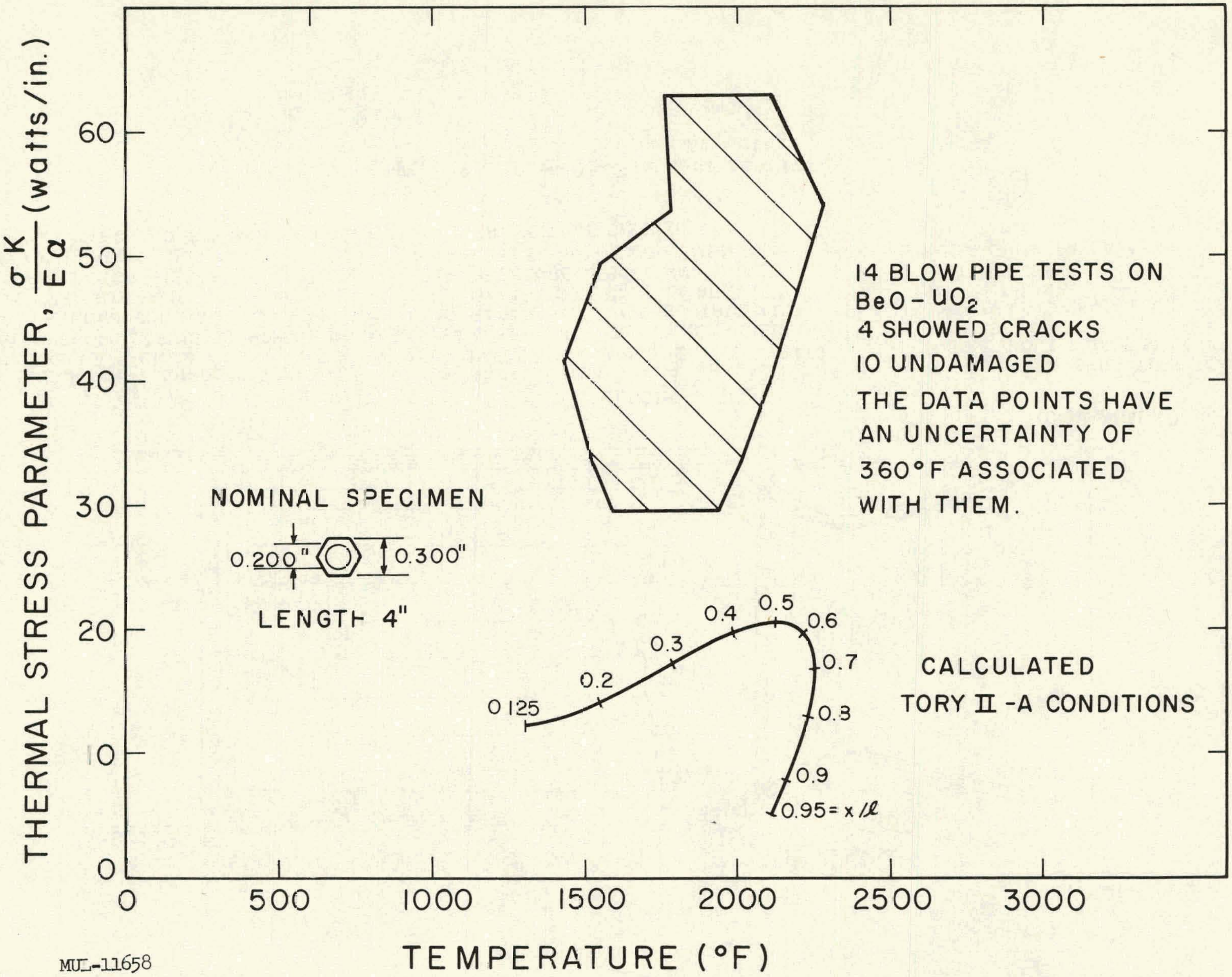

MUL-11658

Fig. 8. Blowpipe thermal stress test results.

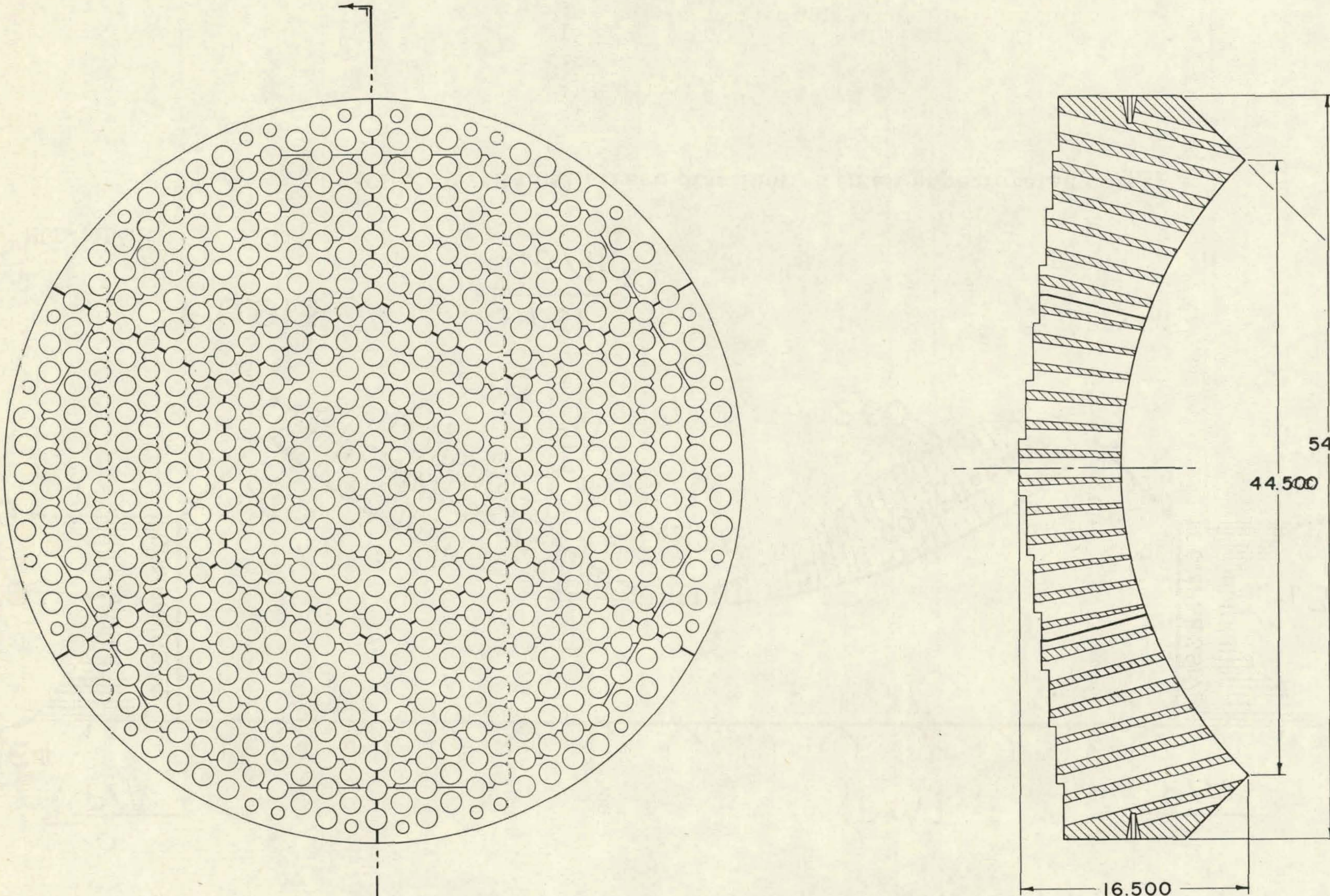

MUL-11659

Fig. 9. Tory II-C-2 dome structure.

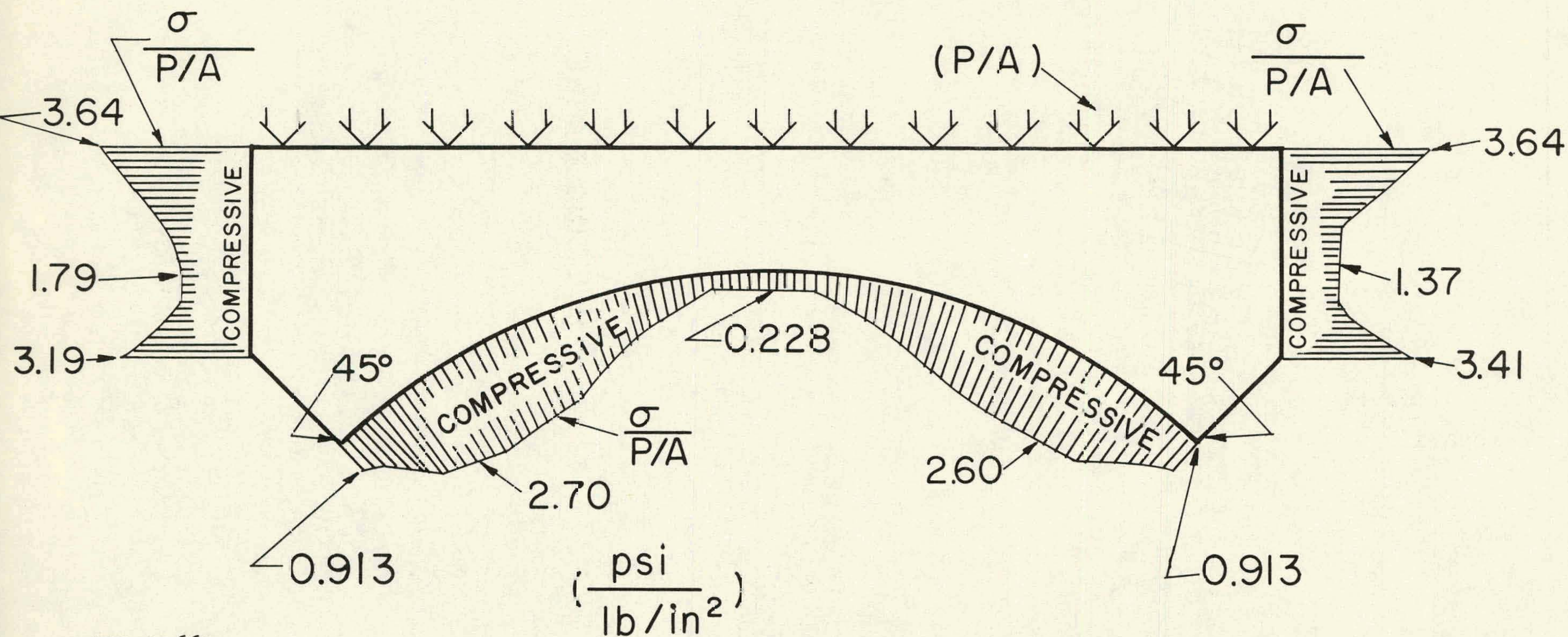

MUL-11660

Fig. 10. Radial stress distribution in an unperforated dome.

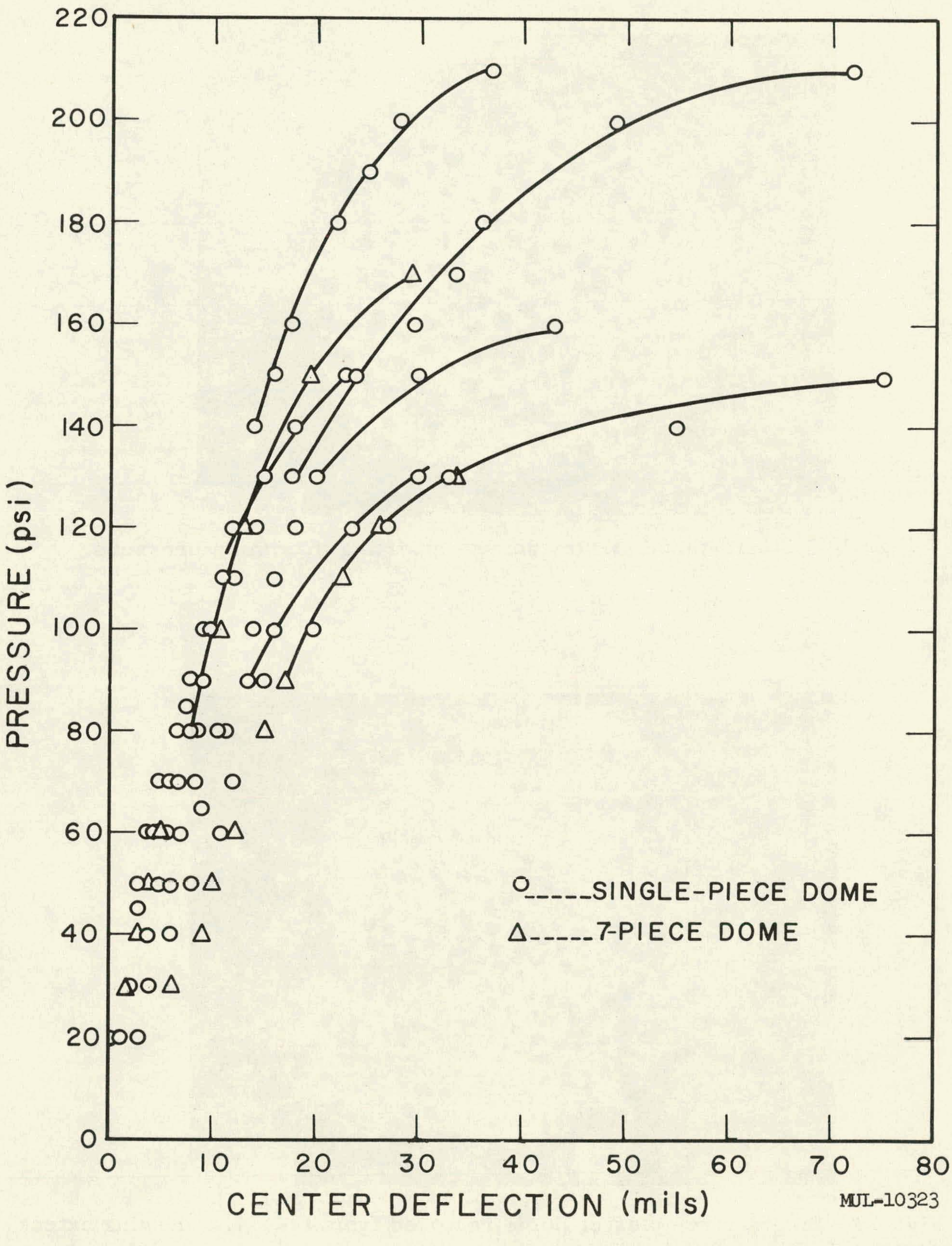

Fig. 11. Pressure vs deflection of perforated plaster domes (50% porosity).

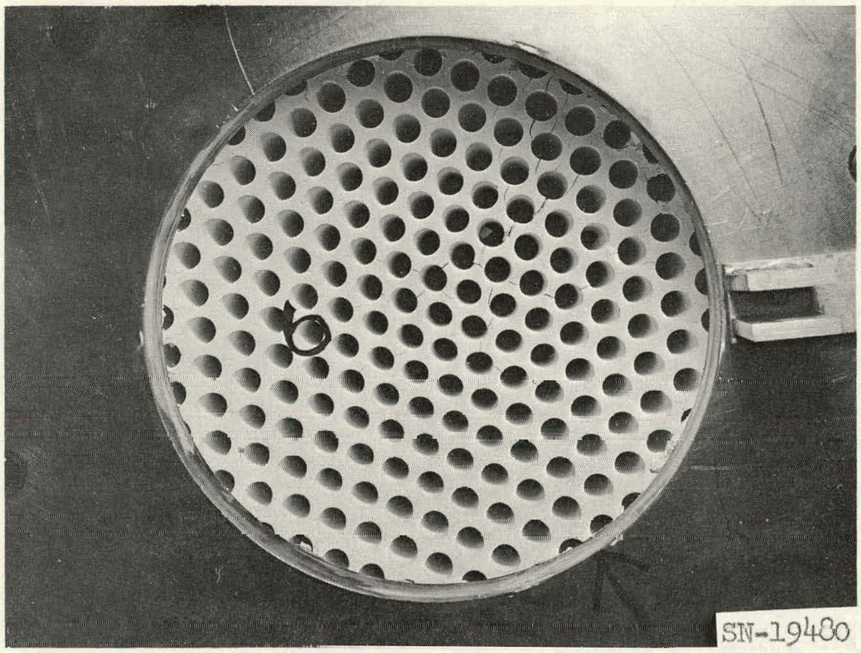

Fig. 12. Single-piece plaster dome supporting maximum pressure.

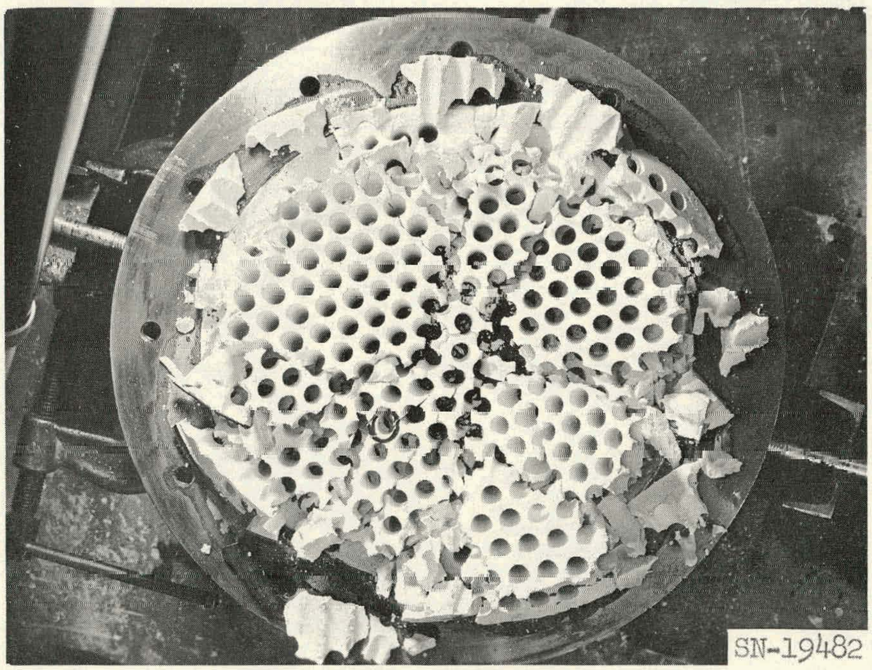

Fig. 13. Single-piece plaster dome removed from test rig, showing extent of damage.

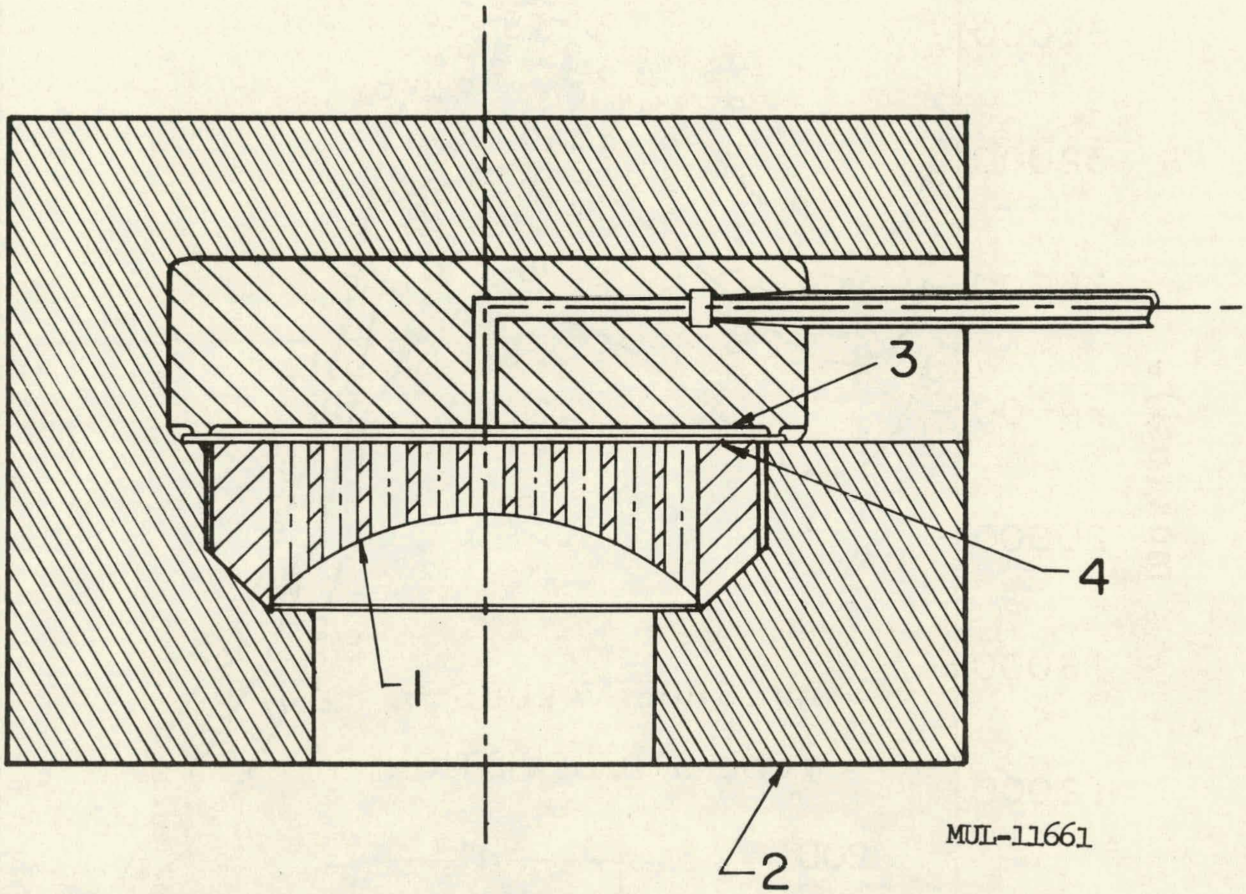

I. SILICON CARBIDE DOME. 2. MOLY BILLET. 3. PRESSURE CHAMBER. 4. MOLY DIAPHRAGM.

Fig. 14. High-temperature test cell.

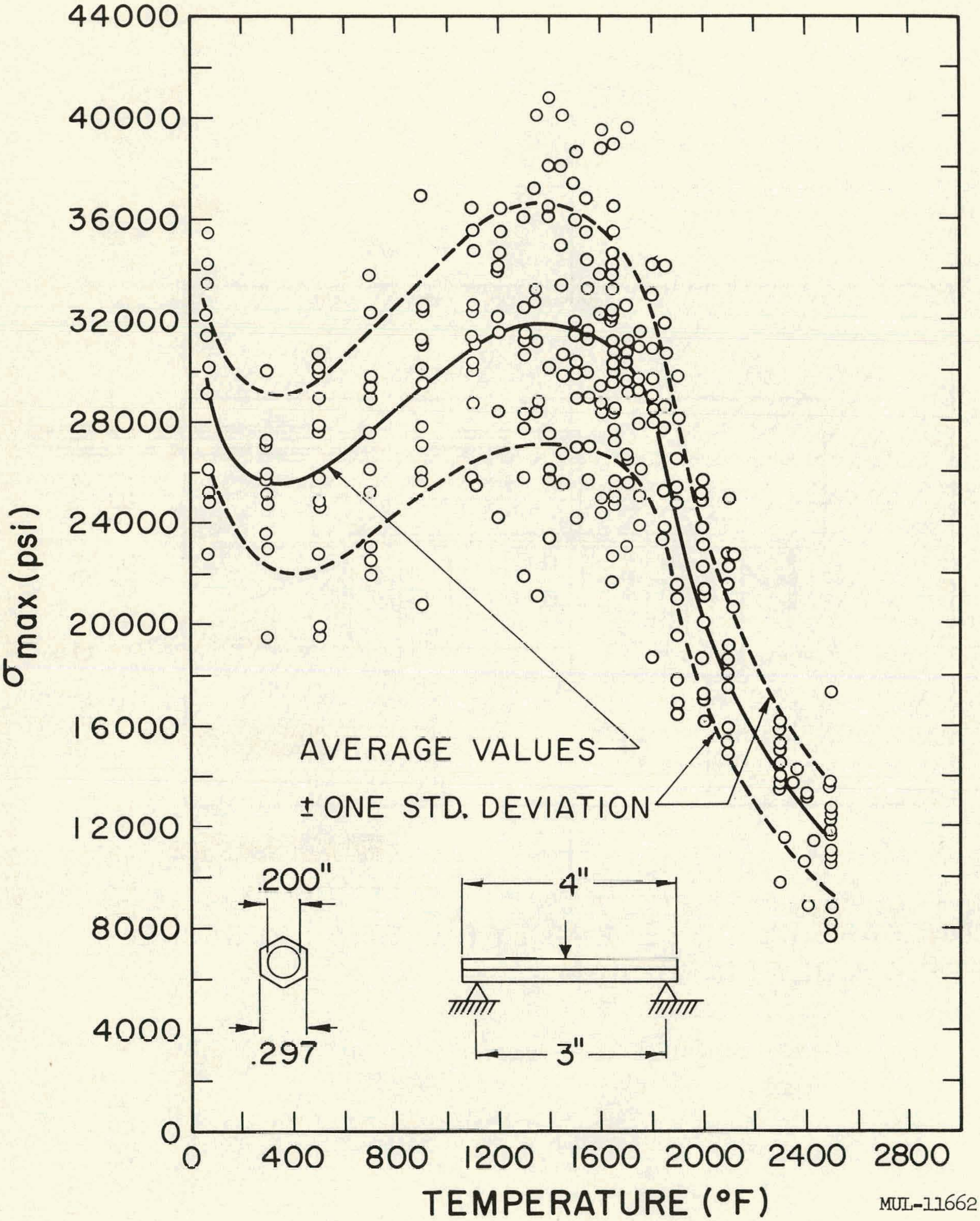

Fig. 15. Modulus of rupture vs temperature.

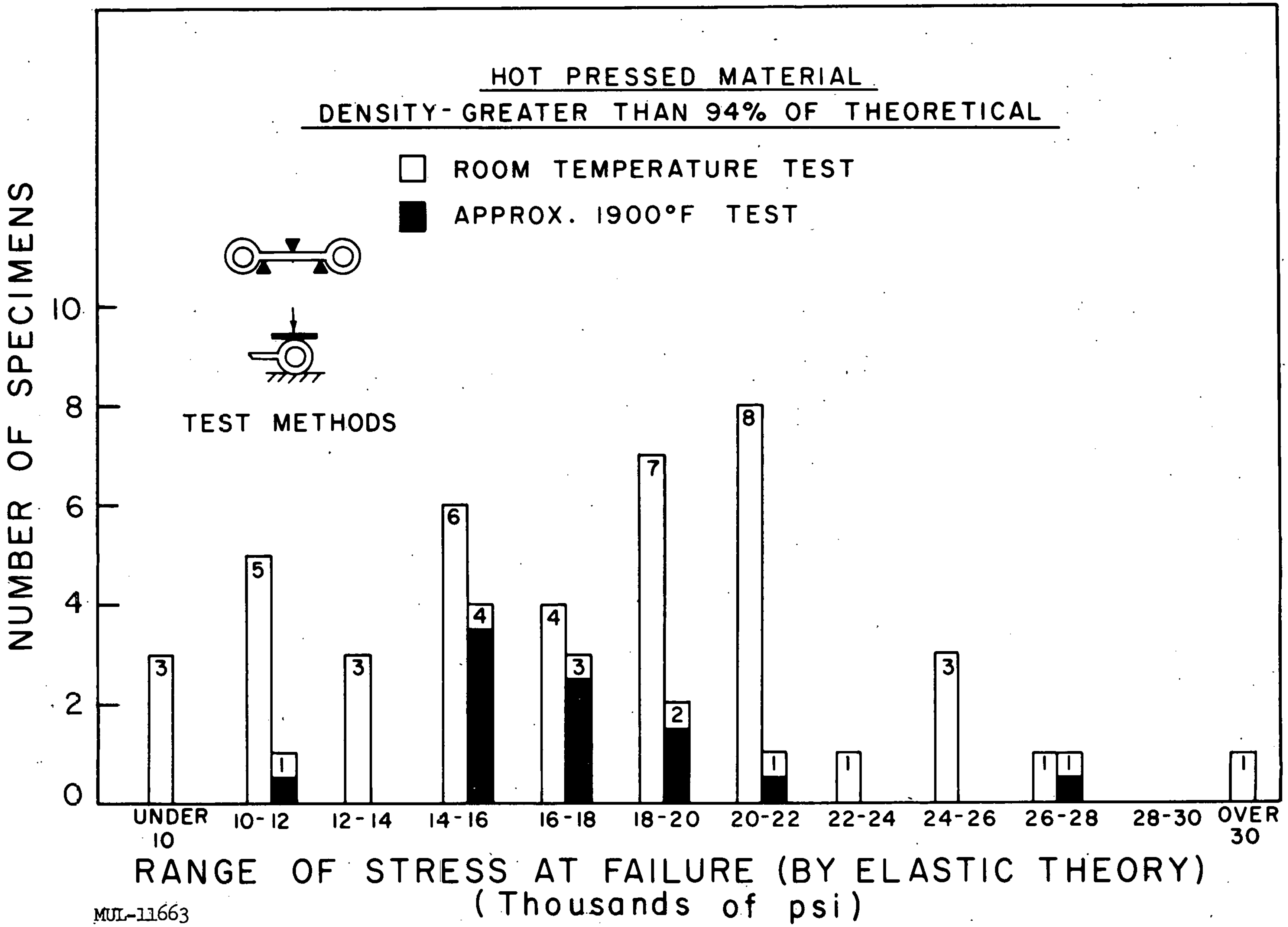

Fig. 16. Strength of beryllium oxide structural links.

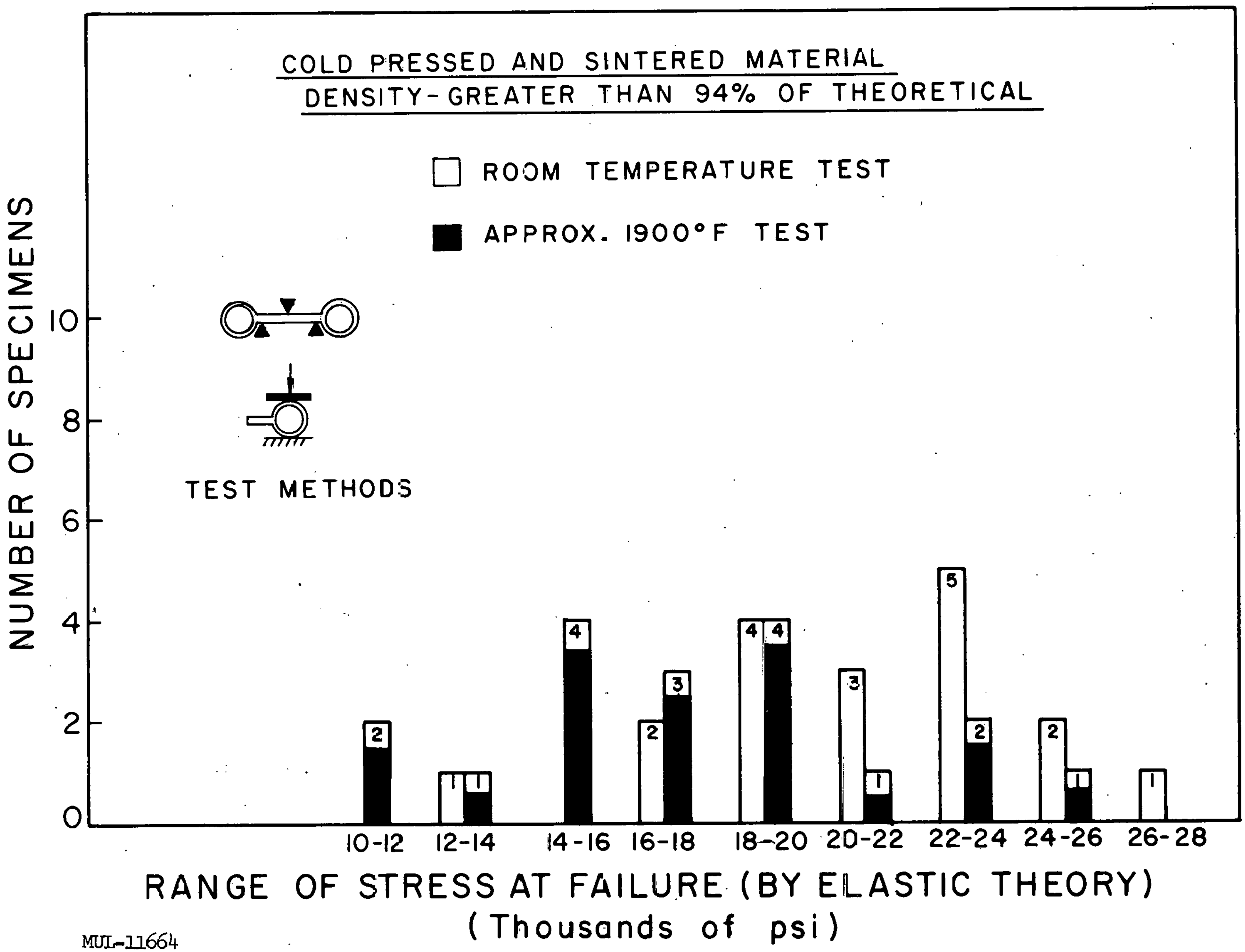

MUL-11664

Fig. 17. Strength of beryllium oxide structural links.

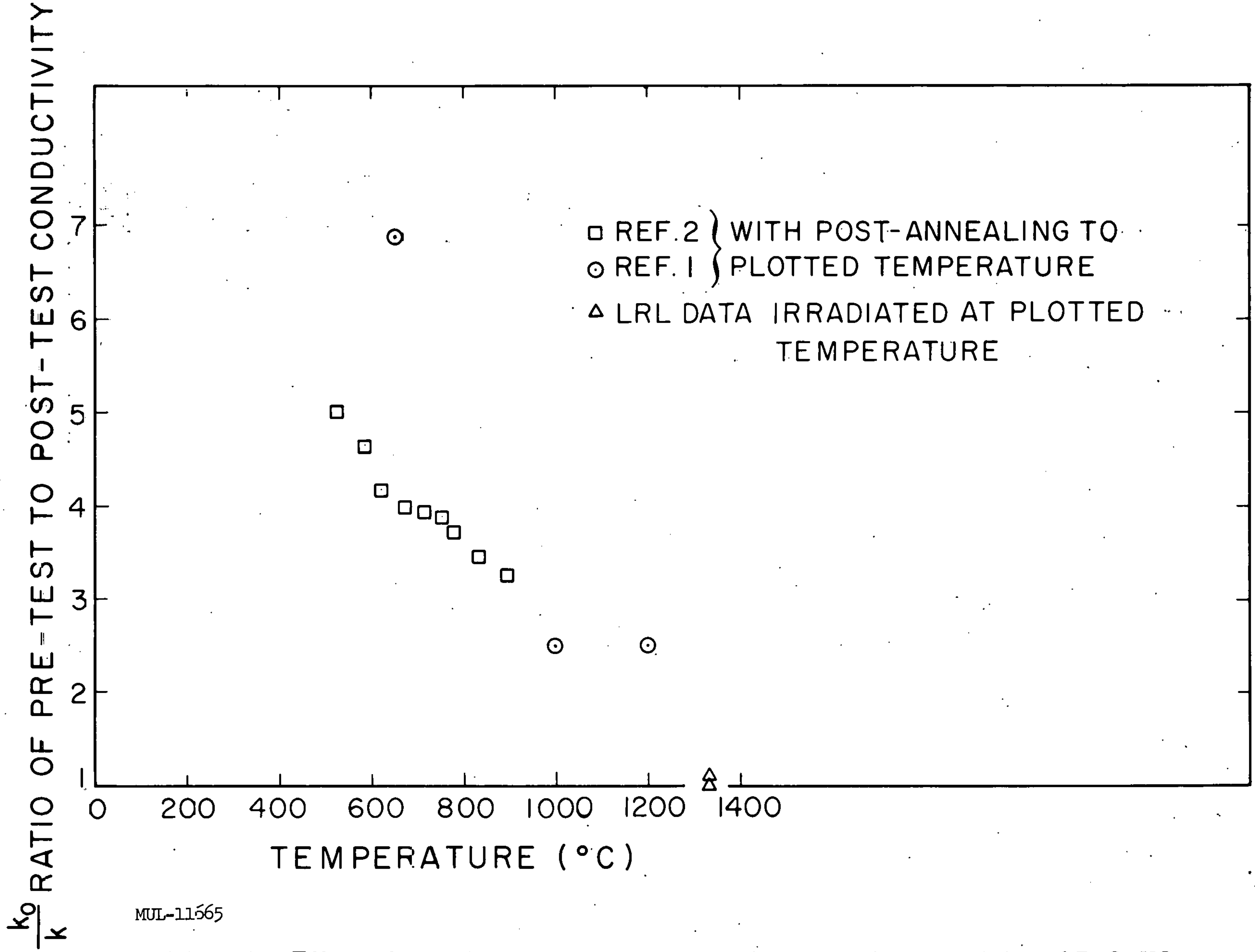

MUL-11565

Fig. 18. Effect of irradiation and temperature on thermal conductivity of BeO-UO_2.

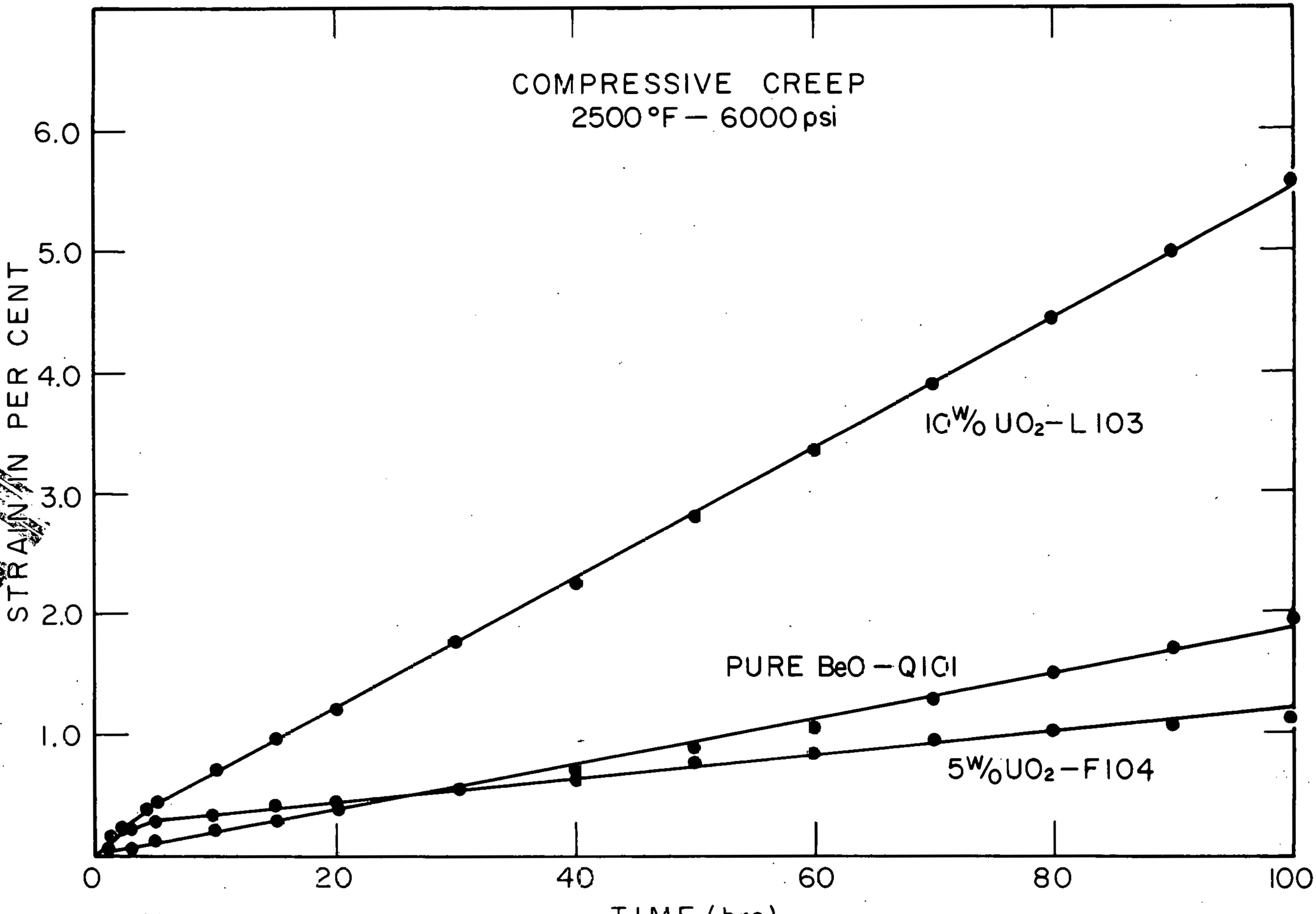

MUL-11194(2)

Fig. 19. Compressive creep of BeO at 2500°F and 6000 psi.